2001

# Time-domain electric-field integral equation with central finite difference

Baek Ho Jung
*Syracuse University*

Tapan Kumar Sarkar
*Syracuse University*

# TIME-DOMAIN ELECTRIC-FIELD INTEGRAL EQUATION WITH CENTRAL FINITE DIFFERENCE

**Baek Ho Jung[1] and Tapan Kumar Sarkar[1]**
[1] Department of Electrical Engineering and Computer Science
Syracuse University
Syracuse, New York 13244

*Received 19 June 2001*

**ABSTRACT:** *In this paper, we present a new formulation using the time-domain electric-field integral equation (TD–EFIE) to obtain a transient scattering response from arbitrarily shaped conducting bodies. The time derivative of the magnetic vector potential is approximated with a central finite difference, and the scalar potential is time averaged by dividing it into two terms. This approach with an implicit method using central-difference results in accurate and stable transient scattering responses from conducting objects. Detailed mathematical steps are included, and several numerical results are presented.* © 2001 John Wiley & Sons, Inc. Microwave Opt Technol Lett 31: 429–435, 2001.

**Key words:** *time-domain electromagnetics; integral equation; finite-difference methods*

## 1. INTRODUCTION

In recent years, several formulations have been presented for the solution of the time-domain integral equation to calculate the electromagnetic scattering from arbitrarily shaped, three-dimensional structures using triangular patch modeling techniques [1]. In an EFIE, there is a time derivative of a magnetic vector potential. By differentiating the EFIE with respect to time, this term is approximated by second-order finite differences, and an explicit solution has been presented [2]. But the results become unstable for late times. Its late-time oscillations could be eliminated by approximating the average value of the current [3]. In this method, the incident field is also differentiated. The disadvantage of this procedure is that an impulse or step function for the incident field cannot be used as an excitation. In addition, to overcome this, a backward finite-difference approximation for the magnetic vector potential term has been presented for the explicit technique [4]. And many numerical results using an explicit method with forward difference and backward difference have been shown in [1, 5, 6]. Recently, an implicit scheme has been proposed to solve two- or three-dimensional scattering problems [7–9].

When one uses an explicit method, the time step becomes very small, and the computed time-domain response becomes unstable with the accumulation of numerical errors before one has computed a sufficiently long response, and it takes much computation time. When an implicit method is used, the time step is larger than that for the explicit case. Therefore, numerical errors due to the approximation of a time derivative using finite difference are increased. In order to overcome this, we develop a new EFIE formulation with a central finite-difference methodology which is more accurate and provides stable solutions.

This paper is organized as follows. In the next section, we briefly describe the general time-domain integral-equation formulation. In Section 3, a TD–EFIE formulation with central finite difference is presented. In Section 4, a numerical solution is presented in detail. In Section 5, we present a matrix equation for the implicit scheme. In Section 6, we show the numerical results for three-dimensional conducting structures, and compare the results with the various EFIE formulations using the backward-difference scheme along with the inverse Fourier transform of the frequency-domain result to obtain the time-domain solution. Lastly, in Section 7, we present some conclusions based on this work.

## 2. GENERAL TD – EFIE

Let $S$ denote a perfectly conducting surface, which may be closed or open, illuminated by a transient electromagnetic wave. This incident wave induces a surface current $\underline{J}(\underline{r}, t)$, on $S$ which then reradiates. We have

$$\underline{E}^s(\underline{J}) = -\frac{\partial \underline{A}}{\partial t} - \nabla\phi \tag{1}$$

where $\underline{A}$ and $\phi$ are the magnetic vector potential and the electric scalar potential given by

$$\underline{A}(\underline{r}, t) = \frac{\mu}{4\pi}\int_S \frac{\underline{J}(\underline{r}', \tau)}{R}\, dS' \tag{2}$$

$$\phi(\underline{r}, t) = \frac{1}{4\pi\varepsilon}\int_S \frac{q(\underline{r}', \tau)}{R}\, dS' \tag{3}$$

$$\tau = t - \frac{R}{c} \tag{4}$$

$$R = |\underline{r} - \underline{r}'| \tag{5}$$

and where $\mu$ and $\varepsilon$ are the permeability and permittivity of space, $c$ is the velocity of wave propagation in that space, and $\underline{r}$ and $\underline{r}'$ are the arbitrarily located observation point and source point. The surface-charge density $q$ is related to the surface divergence of $\underline{J}$ through the equation of continuity:

$$\nabla\cdot\underline{J}(\underline{r}, t) = -\frac{\partial q(\underline{r}, t)}{\partial t} \text{ or } q(\underline{r}, t) = -\int_0^t \nabla\cdot\underline{J}(\underline{r}, t')dt'. \tag{6}$$

Utilizing (6), we have from (3)

$$\phi(\underline{r}, t) = -\frac{1}{4\pi\varepsilon}\int_S\int_0^\tau \frac{\nabla'\cdot\underline{J}(\underline{r}', t')}{R}\, dt'\, dS'. \tag{7}$$

Since the total tangential electric field is zero on the conducting surface for all times, we have

$$[\underline{E}^i + \underline{E}^s(\underline{J})]_{\tan} = 0, \qquad \underline{r} \in S \tag{8}$$

and

$$\left[\frac{\partial \underline{A}}{\partial t} + \nabla\phi\right]_{\tan} = [\underline{E}^i]_{\tan}, \qquad \underline{r} \in S \tag{9}$$

where $\underline{E}^i$ is the incident electric field on the scatterer and the subscript "tan" denotes the tangential component. Equation (9) with (2) and (7) constitutes a TD–EFIE from which the unknown current $\underline{J}(\underline{r}, t)$ may be determined.

## 3. TD – EFIE WITH CENTRAL FINITE DIFFERENCE

For the numerical solution of the TD–EFIE, we divide the time axis into equal intervals of segment $\Delta t$, and define $t_i = i\Delta t$. Approximating the time derivative in (9) by the forward-difference approximation, we can rewrite (9) at $t =$

$t_{i-1}$ as

$$\left[\frac{\underline{A}(\underline{r},t_i)-\underline{A}(\underline{r},t_{i-1})}{\Delta t}+\nabla\phi(\underline{r},t_{i-1})\right]_{\tan}=[\underline{E}^i(\underline{r},t_{i-1})]_{\tan}. \tag{10}$$

Notice that this scheme was used as an explicit method to solving the TD–EFIE [1]. Next, we use the backward difference in (9) at $t = t_i$ as

$$\left[\frac{\underline{A}(\underline{r},t_i)-\underline{A}(\underline{r},t_{i-1})}{\Delta t}+\nabla\phi(\underline{r},t_i)\right]_{\tan}=[\underline{E}^i(\underline{r},t_i)]_{\tan} \tag{11}$$

which is now proposed for the explicit and implicit solutions of a TD–EFIE [4, 8].

We now present a new formulation to improve the accuracy and stability of the implicit solution. We write (9) at time $t = t_{i-1/2}$ as follows:

$$\left[\frac{\underline{A}(\underline{r},t_i)-\underline{A}(\underline{r},t_{i-1})}{\Delta t}+\frac{\nabla\phi(\underline{r},t_i)+\nabla\phi(\underline{r},t_{i-1})}{2}\right]_{\tan}=\left[\underline{E}^i(\underline{r},t_{i-1/2})\right]_{\tan} \tag{12}$$

where we use the central finite difference for the time derivative associated with the vector potential term and the time averaging for the scalar potential term. We combine all three equations (10)–(12) into a unified one so as to use the same code for implementing the various time-differentiating scheme by

$$\left[\frac{\underline{A}(\underline{r},t_i)-\underline{A}(\underline{r},t_{i-1})}{\Delta t}+(1-\nu)\nabla\phi(\underline{r},t_i)+\nu\nabla\phi(\underline{r},t_{i-1})\right]_{\tan}=[\underline{E}^i(\underline{r},t_{i-\nu})]_{\tan} \tag{13}$$

where $\nu = 1$ for the forward, $\nu = 0$ for the backward, and $\nu = 1/2$ for the central finite-difference approximation of the derivative for the magnetic vector potential.

## 4. TESTING PROCEDURE

The structure to be analyzed is approximated by planar triangular patches. The triangular patches have the ability to conform to any geometrical surface of the boundary. As in [10], we define the vector basis function associated with the $n$th edge as

$$\underline{f}_n(\underline{r})=\underline{f}_n^+(\underline{r})+\underline{f}_n^-(\underline{r}) \tag{14}$$

$$\underline{f}_n^{\pm}(\underline{r})=\begin{cases}\dfrac{l_n}{2A_n}\underline{\rho}_n^{\pm}, & \underline{r}\in T_n^{\pm}\\ 0, & \underline{r}\notin T_n^{\pm}\end{cases} \tag{15}$$

where $l_n$ and $A_n$ are the length of the edge and the area of the triangle $T_n^{\pm}$, respectively. $\underline{\rho}_n^{\pm}$ is the position vector defined with respect to the free vertex of $T_n^{\pm}$.

The electric current $\underline{J}$ on the scattering structure may be approximated in terms of the basis functions as

$$\underline{J}(\underline{r},t)=\sum_{n=1}^{N}I_n(t)\underline{f}_n(\underline{r}) \tag{16}$$

where $N$ represent the number of common edges.

We now solve (13) by applying Galerkin's method in the MoM context, and hence the testing functions are the same as the expansion functions. By choosing the expansion functions $\underline{f}_m$ also as the testing functions, and defining the inner product for the two real vector functions $\underline{f}$ and $\underline{g}$ by $\langle \underline{f},\underline{g}\rangle = \int_S \underline{f}\cdot\underline{g}\,dS$, we have from (13)

$$A_m(t_i)+\Delta t(1-\nu)\phi_m(t_i)=\Delta tV_m(t_{i-\nu})+A_m(t_{i-1})+\Delta t\nu\phi_m(t_{i-1}) \tag{17}$$

where

$$A_m(t_i)=\langle \underline{f}_m,\underline{A}(\underline{r},t_i)\rangle \tag{18}$$

$$\phi_m(t_i)=\langle \underline{f}_m,\nabla\phi(\underline{r},t_i)\rangle \tag{19}$$

$$V_m(t_i)=\langle \underline{f}_m,\underline{E}^i(\underline{r},t_i)\rangle. \tag{20}$$

Note that both sides of (17) include the vector and the scalar potential terms, and the left-hand side of (17) contains all of the terms at $t = t_i$.

The next step in the MoM procedure is to substitute the current expansion functions defined in (16) into (18) and (19), and this procedure yields the following equations given by

$$A_m(t_i)=\sum_{n=1}^{N}[A_{mn}^{++}I_n(\tau_{mn}^{++})+A_{mn}^{+-}I_n(\tau_{mn}^{+-})+A_{mn}^{-+}I_n(\tau_{mn}^{-+})+A_{mn}^{--}I_n(\tau_{mn}^{--})] \tag{21}$$

$$\phi_m(t_i)=\sum_{n=1}^{N}[\phi_{mn}^{++}Q_n(\tau_{mn}^{+-})+\phi_{mn}^{+-}Q_n(\tau_{mn}^{+-})+\phi_{mn}^{-+}Q_n(\tau_{mn}^{-+})+\phi_{mn}^{--}Q_n(\tau_{mn}^{--})] \tag{22}$$

where

$$A_{mn}^{pq}=\frac{\mu}{4\pi}\int_S\underline{f}_m^p(\underline{r})\cdot\int_S\frac{\underline{f}_n^q(\underline{r}')}{R}\,dS'\,dS \tag{23}$$

$$\phi_{mn}^{pq}=\frac{1}{4\pi\varepsilon}\int_S\nabla\cdot\underline{f}_m^p(\underline{r})\int_S\frac{\nabla'\cdot\underline{f}_m^q(\underline{r}')}{R}\,dS'\,dS \tag{24}$$

$$I_n(\tau_{mn}^{pq})=I_n\left(t_i-\frac{R_{mn}^{pq}}{c}\right) \tag{25}$$

$$Q_n(\tau_{mn}^{pq})=\int_0^{\tau_{mn}^{pq}}I_n(t')dt' \tag{26}$$

$$\tau_{mn}^{pq}=t_i-\frac{R_{mn}^{pq}}{c},\ R_{mn}^{pq}=|\underline{r}_m^{cp}-\underline{r}_n^{cp}| \tag{27}$$

where $p$ and $q$ are $+$ or $-$, and $\underline{r}_m^{cp}$ is the position vector of the centroid in triangle $T_m^p$. In deriving (21) and (22), we assumed $t_i-(R/c)\approx t_i-(R_{mn}^{pq}/c)$. If the integrals on the unprimed variables in (23) and (24) are evaluated by approximating the integrand by the respective values at the centroids

of the testing triangles $T_m^p$, (23) and (24) become

$$A_{mn}^{pq} = \frac{\mu l_m l_n}{16\pi} \underline{\rho}_m^{cp} \cdot \frac{1}{A_n^q} \int_{T_n^q} \frac{\underline{\rho}_n^q}{R_m^p} \, dS' \tag{28}$$

$$\phi_{mn}^{pq} = \frac{l_m l_n}{4\pi\varepsilon} \frac{1}{A_n^q} \int_{T_n^q} \frac{1}{R_m^p} \, dS' \tag{29}$$

where

$$R_m^p = |\underline{r}_m^{cp} - \underline{r}'|. \tag{30}$$

Integrals (28) and (29) may be evaluated by the methods described in [11].

Finally, (20) can be computed by using the similar centroid testing as

$$V_m(t_i) = V_m^+(t_i) + V_m^-(t_i) \tag{31}$$

$$V_m^p(t_i) = \int_S \underline{f}_m^p(\underline{r}) \cdot \underline{E}^i(\underline{r}, t_i) dS \approx \frac{l_m}{2} \underline{\rho}_m^{cp} \cdot \underline{E}^i(\underline{r}_m^{cp}, t_i) \tag{32}$$

where $p$ is + or −.

## 5. MATRIX EQUATIONS FOR IMPLICIT METHOD

Consider the time-dependent current coefficients $I_n$ in (25) and integration of the current coefficient $Q_n$ in (26). We assume the currents as an approximately linear function. When $R_{mn}^{pq} \geq c\Delta t$ or $t_{j-1} < \tau_{mn}^{pq} \leq t_j$, where $t_j \leq t_{i-1}$, (25) and (26) can be rewritten as

$$I_n(\tau_{mn}^{pq}) = (1 - \delta) I_n(t_{j-1}) + \delta I_n(t_j) \tag{33}$$

$$Q_n(\tau_{mn}^{pq}) = \Delta t \sum_{k=0}^{j-2} I_n(t_k) + \frac{\Delta t}{2}(1 + 2\delta - \delta^2) I_n(t_{j-1}) + \frac{\Delta t}{2} \delta^2 I_n(t_j) \tag{34}$$

where

$$\delta = \frac{\tau_{mn}^{pq} - t_{j-1}}{\Delta t}. \tag{35}$$

Using (33) and (34), we can compute (17) at time step $t = t_i$, except terms for which $R_{mn}^{pq} < c\Delta t$. For terms for which $R_{mn}^{pq} < c\Delta t$ or $t_{i-1} < \tau_{mn}^{pq} \leq t_i$, (25) and (26) can be expressed as

$$I_n(\tau_{mn}^{pq}) = S_{mn}^{pq} I_n(t_{i-1}) + (1 - S_{mn}^{pq}) I_n(t_i) \tag{36}$$

$$Q_n(\tau_{mn}^{pq}) = \Delta t \sum_{k=0}^{i-2} I_n(t_k) + \frac{\Delta t}{2}\left(2 - S_{mn}^{pq^2}\right) I_n(t_{i-1}) + \frac{\Delta t}{2}(1 - S_{mn}^{pq})^2 I_n(t_i) \tag{37}$$

where

$$S_{mn}^{pq} = \frac{R_{mn}^{pq}}{c\Delta t}. \tag{38}$$

With (36) and (37), we express (21) and (22) by dividing their terms as

$$A_m(t_i) = \sum_{n=1}^{N} \dot{X}_{mn} I_n(t_i) + \dot{P}_m(t_{i-1}) + \tilde{A}_m(t_i) \tag{39}$$

$$\phi_m(t_i) = \sum_{n=1}^{N} \dot{Y}_{mn} I_n(t_i) + \dot{B}_m(t_{i-1}) + \dot{D}_m(t_{i-2}) + \tilde{\phi}_m(t_i) \tag{40}$$

where

$$\dot{X}_{mn} = A_{mn}^{++}(1 - S_{mn}^{++}) + A_{mn}^{+-}(1 - S_{mn}^{+-}) + A_{mn}^{-+}(1 - S_{mn}^{-+}) + A_{mn}^{--}(1 - S_{mn}^{--}) \tag{41}$$

$$\dot{P}_m(t_{i-1}) = \sum_{n=1}^{N} (A_{mn}^{++} S_{mn}^{++} + A_{mn}^{+-} S_{mn}^{+-} + A_{mn}^{-+} S_{mn}^{-+} + A_{mn}^{--} S_{mn}^{--}) I_n(t_{i-1}) \tag{42}$$

$$\dot{Y}_{mn} = \frac{\Delta t}{2}\left[ \phi_{mn}^{++}(1 - S_{mn}^{++})^2 + \phi_{mn}^{+-}(1 - S_{mn}^{+-})^2 + \phi_{mn}^{-+}(1 - S_{mn}^{-+})^2 + \phi_{mn}^{--}(1 - S_{mn}^{--})^2 \right] \tag{43}$$

$$\dot{B}_m(t_{i-i}) = \frac{\Delta t}{2} \sum_{n=1}^{N} \left[ \phi_{mn}^{++}\left(2 - S_{mn}^{++^2}\right) + \phi_{mn}^{+-}\left(2 - S_{mn}^{+-^2}\right) + \phi_{mn}^{-+}\left(2 - S_{mn}^{-+^2}\right) + \phi_{mn}^{--}\left(2 - S_{mn}^{--^2}\right) \right] I_n(t_{i-1}) \tag{44}$$

$$\dot{D}_m(t_{i-2}) = \Delta t \sum_{n=1}^{N} \left[ (\phi_{mn}^{++} + \phi_{mn}^{+-} + \phi_{mn}^{-+} + \phi_{mn}^{--}) \times \sum_{k=0}^{i-2} I_n(t_k) \right]. \tag{45}$$

In (39)–(45), the dot sign symbol on top of the expressions implies that $R_{mn}^{pq} < c\Delta t$ for the elements, and the tilde sign on top of the expressions implies that $R_{mn}^{pq} \geq c\Delta t$ for the elements. Therefore, $\tilde{A}_m(t_i)$ in (39) and $\tilde{\phi}_m(t_i)$ in (40) are of the same form as (21) and (22), respectively, for each $R_{mn}^{pq} \geq c\Delta t$.

Substituting (39) and (40) into (17), we can obtain a matrix equation as follows:

$$[\alpha_{mn}][I_n(t_i)] = [\beta_m] \tag{46}$$

where

$$\alpha_{mn} = \dot{X}_{mn} + \Delta t(1 - \nu)\dot{Y}_{mn} \tag{47}$$

$$\beta_m = \Delta t V_m(t_{i-\nu}) + A_m(t_{i-1}) - [\tilde{A}_m(t_i) - \dot{P}_m(t_{i-1})] - \Delta t \nu \phi_m(t_{i-1}) - \Delta t(1 - \nu)[\tilde{\phi}_m(t_i) + \dot{B}_m(t_{i-1}) + \dot{D}_m(t_{i-2})]. \tag{48}$$

We note that, when $\nu = 1$ for the forward-difference case, the scalar potential term does not contribute to $\alpha_{mn}$ in (47) and the last term of $\beta_m$ in (48). When $\nu = 0$ for the backward-difference approximation of the derivative, the scalar potential term does not contribute to the fourth term of $\beta_m$ in (48). When $\nu = 1/2$ for the central-difference case, the scalar potential contributes to both the matrices $[\alpha_{mn}]$ and $[\beta_m]$. And the incident field is also considered at the midpoint of each time step. Matrix $[\alpha_{mn}]$ is not a function of time, and hence the inverse of the matrix needs to be computed only once at the beginning of the computation step.

## 6. NUMERICAL RESULTS

In this section, we present some numerical results for selected scatterers, although the algorithm has been tested for several geometrical shapes. Here, we present the currents induced on a flat plate, cube, and sphere using a backward- ($\nu = 0$) and a central-difference ($\nu = 1/2$) scheme. We do not show the result for the forward-difference formula ($\nu = 1$) because of its early-time oscillations. As a first example, consider a flat, 2 m $\times$ 2 m square plate, located in the $xy$-plane shown in Figure 1. Eight divisions were made along the $x$-direction and seven along the $y$-direction, resulting in 112 triangular patches with 153 common edges, and $R_{\min} =$ 12.65 cm, where $R_{\min}$ represents the minimum distance between any two patches. It is illuminated by a sinusoidal plane wave, given by

$$\underline{E}^i(\underline{r}, t) = \underline{E}_0 \sin \omega\left(t - \frac{\underline{r} \cdot \hat{k}}{c}\right) \tag{49}$$

with $\underline{E}_0 = \hat{x}$, $\omega = 2\pi f$, and $f = 50$ MHz. $\hat{k}$ is the unit propagation vector. The field is incident from $\phi = 0°$ and $\theta = 0°$. The time step is chosen so that $c\Delta t = 2R_{\min}$ in order to generate the implicit solution. Figure 2 shows the transient response for an $x$-directed current at the center of the conducting plate shown in Figure 1 illuminated by a sinusoidal wave using the backward- and central-difference scheme until 100 lm (light meter). We can see that the transient current obtained by an EFIE using the central difference is very stable. But the current obtained by the backward scheme has developed spurious oscillations in the solution after only one period. When steady state is reached in the time domain, the amplitude of the current should correspond in amplitude to a frequency-domain solution when the same plate is excited in the frequency domain by a plane wave of 1 V/m amplitude with a frequency of 50 MHz. In Figure 2, the amplitude of the fourth positive peak is 9.365 mA. When a plane-wave excitation is chosen for the solution of the current on the plate utilizing an EFIE in the frequency domain, the frequency-domain solution yields a value of 9.374 mA/m at the same edge. It therefore validates the time-domain EFIE with central difference, and also the frequency domain EFIE.

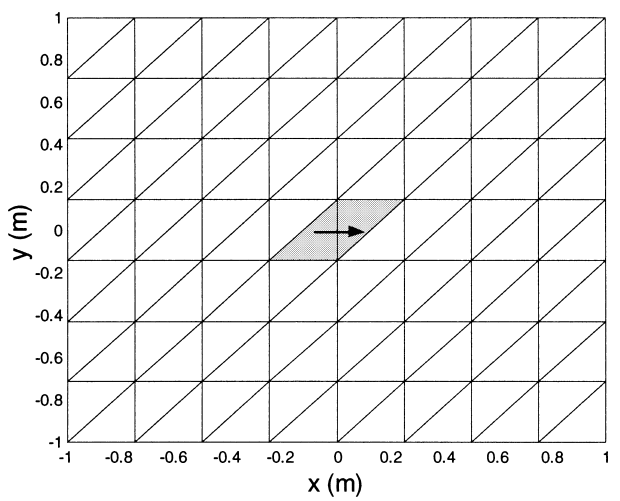


**Figure 1** Triangle patching of a conducting plate (2 m $\times$ 2 m). 112 patches. 153 common edges

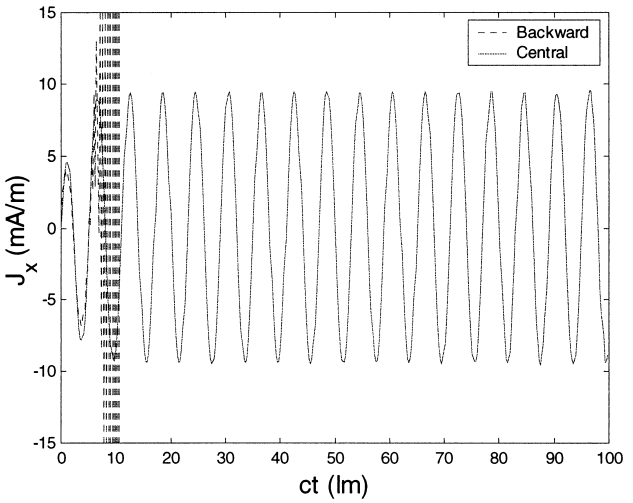


**Figure 2** Transient response of $x$-directed current at the center of conducting plate (Fig. 1) illuminated by a sinusoidal wave with frequency 50 MHz

Next, we present numerical results for the currents from conducting objects when illuminated by a Gaussian plane wave, given by

$$\underline{E}^i(\underline{r}, t) = \underline{E}_0 \frac{4}{\sqrt{\pi}\, T} e^{-\gamma^2} \tag{50}$$

where

$$\gamma = \frac{4}{T}(ct - ct_0 - \underline{r} \cdot \hat{k}) \tag{51}$$

with $\underline{E}_0 = \hat{x}$, $T = 4$ lm, and $ct_0 = 6$ lm. The field is incident from $\phi = 0°$ and $\theta = 0°$. For comparison, we present the results obtained by the inverse discrete Fourier transform of the frequency-domain (IDFT) solution. We first consider the plate in Figure 1. Figure 3 shows the transient response from an $x$-directed current induced at the center of the plate as a function of time obtained by using double- and single-precision computations. It is evident from the figures that the result from the TD–EFIE with central difference is very accurate and stable. Note the absence of any late-time instability in the result, even for single precision. However, for the backward-difference scheme, use of double precision only delays the starting on time for the spurious oscillations.

The second structure is a conducting cube shown in Figure 4, 1 m on a side, centered about the origin. There are four, five, and four subdivisions of the structure along the $x$-, $y$-, and $z$-directions, respectively. This represents a total of 224 patches and 336 common edges. The time step has been chosen as $c\Delta t = 2R_{\min}$, where $R_{\min} = 10.67$ cm. The $x$-directed current at the center of the top face and the $z$-directed current at the center of the side face of the cube are seen in Figures 5 and 6, respectively. Here, the agreement with the frequency-domain data is very good. Even though we are using single precision, the transient response for the current is very stable and accurate.

As a third geometry, Figure 7 shows a conducting sphere of radius 0.5 m centered at the origin. There are eight subdivisions along the $\theta$-directions and 12 subdivisions along the $\phi$-direction. This results in a total of 168 patches and 152 common edges. The time step is chosen as $c\Delta t = 4R_{\min}$,

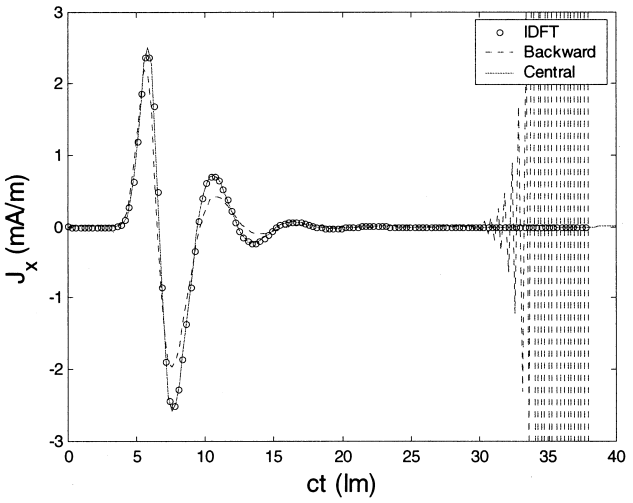


(a)

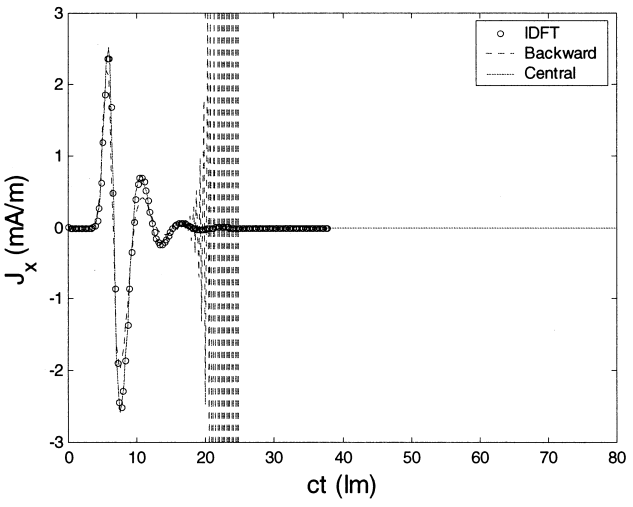


(b)

**Figure 3** Transient response for an $x$-directed current at the center of a conducting plate (Fig. 1). The results have been computed using (a) double precision and (b) single precision

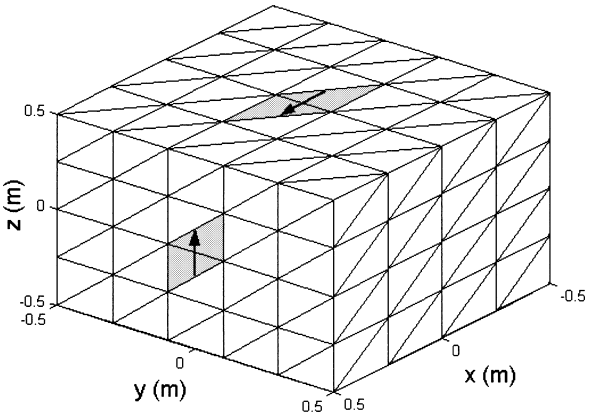


**Figure 4** Triangle patching scheme for a conducting cube (1 m × 1 m × 1 m) with 224 patches having 336 common edges

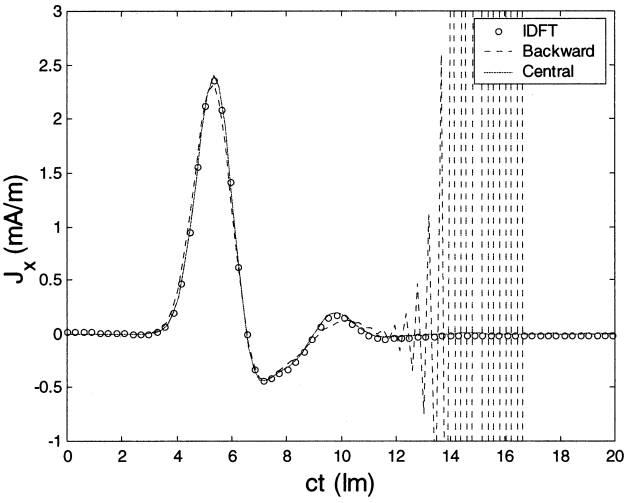


(a)

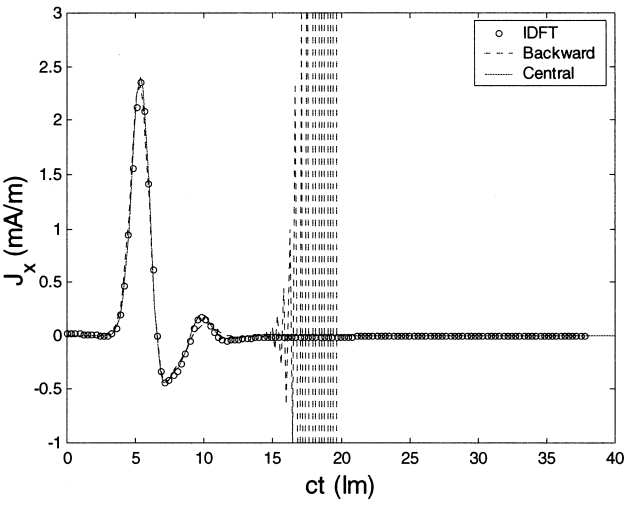


(b)

**Figure 5** Transient response for an $x$-directed current at the center $(0, 0, 0.5)$ of the top face of a conducting cube (Fig. 4). The results have been computed using (a) single precision and (b) double precision

where $R_{\min} = 6.37$ cm. Figure 8 shows the $\theta$-component and $\phi$-component of the currents as indicated by the arrows in Figure 7. The agreement between the results from the EFIE with central difference using single-precision computation and IDFT is very good, but the result from the EFIE with backward difference has late-time oscillations, irrespective of whether single- or double-precision arithmetic is used in the computation.

## 7. CONCLUSION

In this paper, we have presented a new method to obtain the solution to a transient scattering from conducting structures. This time-domain EFIE formulation with an implicit method is derived using a central-difference scheme for the vector potential and a time-averaging technique for the scalar potential. Also, the incident field is evaluated at a midpoint of the time interval. Transient responses computed by the presented method are very accurate and stable, even with single-precision computations.

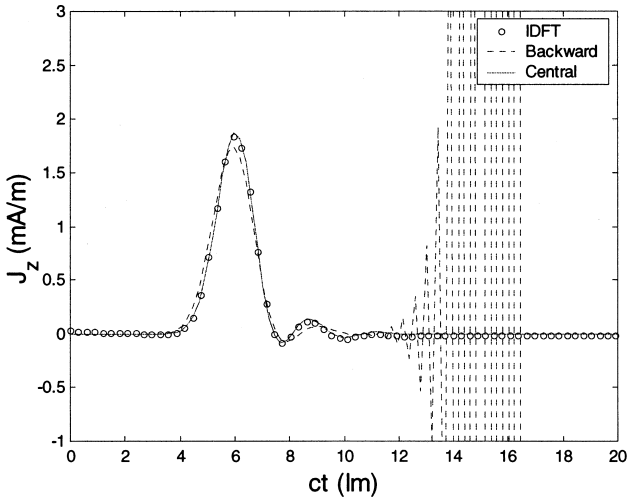


(a)

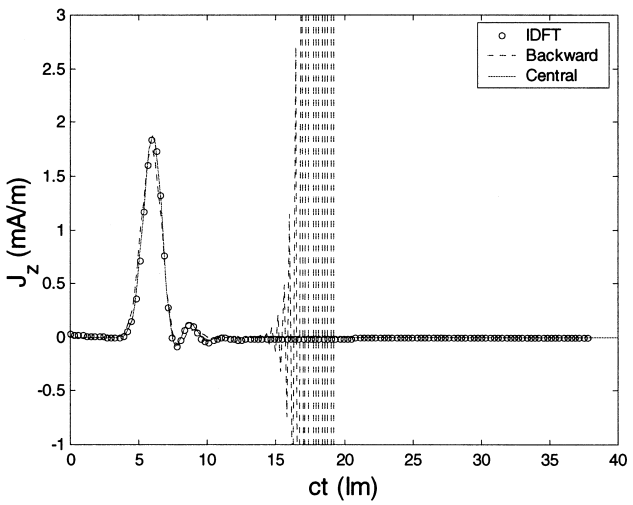


(b)

**Figure 6** Transient response for a $z$-directed current at the center $(0.5, 0, 0)$ of a side face of a conducting cube (Fig. 4). The results have been computed using (a) single precision and (b) double precision

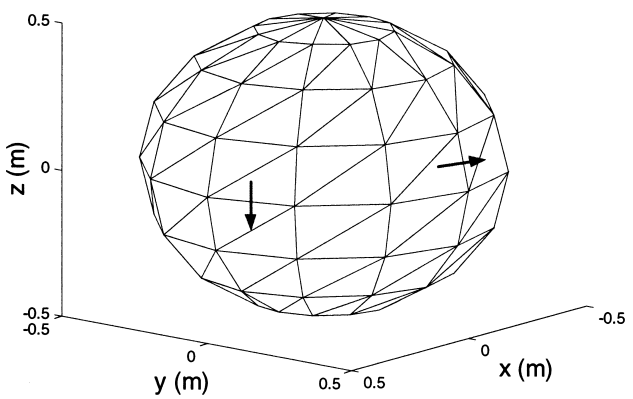


**Figure 7** Triangle patching of a conducting sphere with radius 0.5 m. 168 patches. 152 common edges

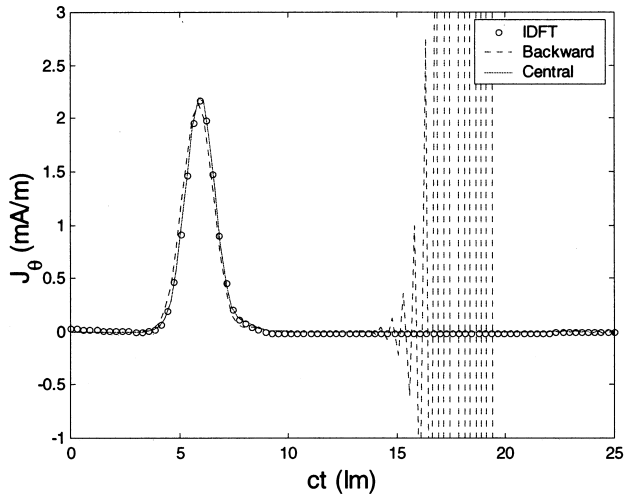


(a)

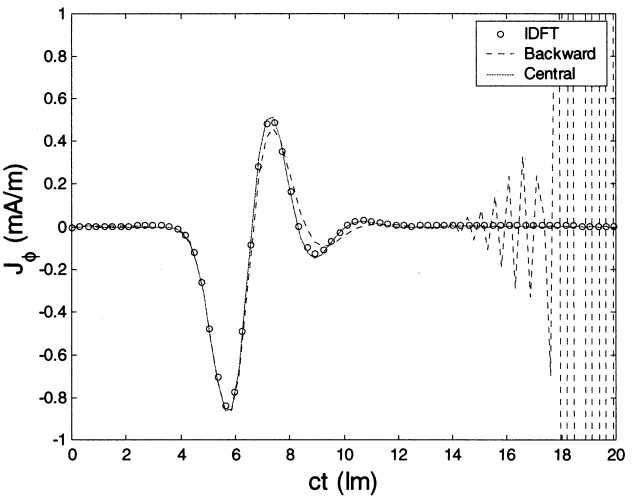


(b)

**Figure 8** Transient response of current on a conducting sphere (Fig. 7). (a) $\theta$-component of current at $\theta = 90°$, $\phi = 15°$. (b) $\phi$-component of current at $\theta = 78.75°$, $\phi = 90°$

## REFERENCES


1. S.M. Rao, Time domain electromagnetics, Academic, New York, 1999.
2. S.M. Rao and D.R. Wilton, Transient scattering by conducting surfaces of arbitrary shape, IEEE Trans Antennas Propagat 39 (1991), 56–61.
3. D.A. Vechinski and S.M. Rao, A stable procedure to calculate the transient scattering by conducting surfaces of arbitrary shape, IEEE Trans Antennas Propagat 40 (1992), 661–665.
4. S.M. Rao and T.K. Sarkar, An alternative version of the time-domain electric field integral equation for arbitrarily shaped conductors, IEEE Trans Antennas Propagat 41 (1993), 831–834.
5. A. Sadigh and E. Arvas, Treating the instabilities in marching-on-in time method from a different perspective, IEEE Trans Antennas Propagat 41 (1993), 1695–1702.
6. P.J. Davies, On the stability of time-marching schemes for the general surface electric-field integral equation, IEEE Trans Antennas Propagat 44 (1996), 1467–1473.
7. S.M. Rao, D.A. Vechinski, and T.K. Sarkar, Transient scattering by conducting cylinders—Implicit solution for the transverse electric case, Microwave Opt Technol Lett 21 (1999), 129–134.
8. S.M. Rao and T.K. Sarkar, An efficient method to evaluate the

time-domain scattering from arbitrarily shaped conducting bodies, Microwave Opt Technol Lett 17 (1998), 321–325.
9. T.K. Sarkar, W. Lee, and S.M. Rao, Analysis of transient scattering from composite arbitrarily shaped complex structures, IEEE Trans Antennas Propagat 48 (2000), 1625–1634.
10. S.M. Rao, D.R. Wilton, and A.W. Glisson, Electromagnetic scattering by surfaces of arbitrary shape, IEEE Trans Antennas Propagat AP-30 (1982), 409–418.
11. D.R. Wilton, S.M. Rao, A.W. Glisson, D.H. Schaubert, O.M. Al-Bundak, and C.M. Butler, Potential integrals for uniform and linear source distributions on polygonal and polyhedral domains, IEEE Trans Antennas Propagat AP-32 (1984), 276–281.



# ON THE ANALYSIS OF A WEAKLY GUIDING DOUBLY CLAD DIELECTRIC OPTICAL FIBER WITH AN ANNULAR CORE

**B. C. Sarkar,[1] P. K. Choudhury,[2] and T. Yoshino[1]**
[1] Department of Electrical Engineering
Faculty of Engineering
Gunma University
Kiryu 376-8515, Gunma, Japan
[2] Satellite Venture Business Laboratory
Faculty of Engineering
Gunma University
Kiryu 376-8515, Gunma, Japan

*Received 26 June 2001*

**ABSTRACT:** *A fairly rigorous analytical treatment of an annular core dielectric optical fiber is presented, the core of the fiber lying between two concentric claddings with the outer cladding extended infinitely. For the theoretical approach, the approximation of the vanishing refractive-index difference between the core and the cladding sections is implemented. The investigation is on the preliminary ground, and a numerical estimation of the modal cutoffs is presented for the said fiber. The effects of the core width as well as the inner core diameter on the propagation constants $\beta_c$ at field cutoffs are presented. Plots are also shown of the variation of $\beta_c$ with the change in the refractive-index values.* © 2001 John Wiley & Sons, Inc. Microwave Opt Technol Lett 31: 435–439, 2001.

**Key words:** *optical fibers; EM wave propagation*

## 1. INTRODUCTION

The study of the propagation of light waves through waveguides under a variety of conditions has always been a subject of great interest among the electromagnetics (EM) community. Several investigators have endeavored to the study of waveguides having various forms of cross sections, yielding important and interesting results. A few examples are elliptical fibers [1, 2], rectangular [3, 4], triangular [5, 6], parabolic cylindrical [7–9], polygonal [10], and Piet Hein [11, 12] type guides.

Analyses of doubly clad fibers have been presented by Kawakami and Nishida [13] and Chaubey et al. [14], where the innermost section of the fiber was considered to be the fiber core. Further, multiple-clad fibers are used in designing dispersion-flattened fibers having low dispersion over a relatively large wavelength range of 1.3–1.6 $\mu$m [15]. These fibers are indispensable in long-distance optical communications. In this connection, fibers with an annular core would be interesting, and may present some technological applications. In the present paper, we report only a preliminary analytical study of the propagation characteristics of a doubly clad step-index dielectric optical fiber, where the core is a dielectric annulus lying between two claddings of the same material having their refractive-index (RI) values slightly less than that of the core section. The resulting fiber structure may be called an annular core fiber (AFC). A small difference between the refractive indexes allows the use of the scalar field approximation [16]. This makes the analysis a bit easier, and to some extent, it is necessary too because a strict analytical approach becomes forbiddingly difficult due to the presence of multiple layers. An attempt is made to study the characteristic equations and the cutoff behavior of AFCs, and the results are compared with previously published works [13, 14] on doubly clad optical fibers. Although part of the analysis is well known and goes on in a more or less equivalent form, we believe that the study gives us an important insight into the general modal behavior of annular fibers with respect to their field cutoffs. The structure of the ACF under consideration certainly has a kind of periodicity, and one potential application of such materials is a type of optical waveguide where light is confined by surrounding it with a bandgap material [17]. Moreover, a narrowband spectral filtering aspect of such fibers with step-index or *W*-index fibers may also be expected [18].

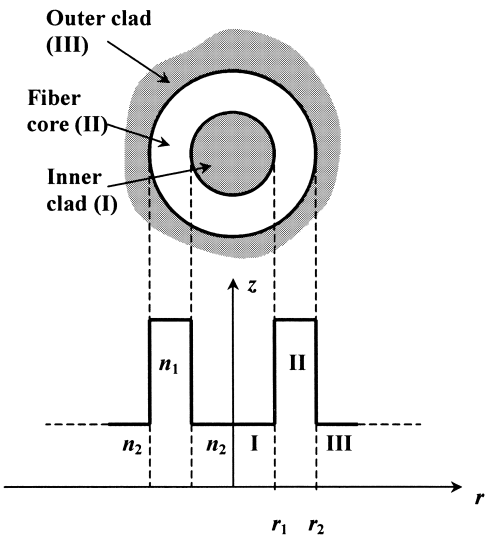


**Figure 1** Transverse view of AFC and the RI profile

## 2. FORMULATION

Figure 1 shows the transverse cross-sectional view of ACF, and the RI profile, the annulus being the guiding region having RI $n_1$ covered with two concentric claddings of the same RI $n_2$ such that $(n_1 - n_2)/n_1 \ll n_1$. The index difference is assumed to be very small so that the weak guidance approximation [16] can be well applicable to the case. We use the cylindrical polar coordinate system $(r, \phi, z)$. Considering the field $\psi$ to be harmonic in time $t$ and coordinate $z$, it can be expressed as

$$\psi(r, \phi, z, t) = \psi_0 \exp\{-j(\omega t - \beta z)\} \exp(j\nu\phi). \quad (1)$$

Here, $\psi$ represents the electric/magnetic field, $\omega$ is the angular frequency, $\nu$ is a mode-designation index, and $\beta$ is the propagation constant along the axial direction. Equation

# CORRECTIONS TO "TIME-DOMAIN ELECTRIC-FIELD INTEGRAL EQUATION WITH CENTRAL FINITE DIFFERENCE"

**Baek Ho Jung[1] and Tapan Kumar Sarkar[2]**
[1] Department of Information and Communication Engineering
Hoseo University
Asan 336-795, Korea
[2] Department of Electrical Engineering and Computer Science
Syracuse University
Syracuse, New York 13244

*Received 11 May 2001*
Originally published Microwave Opt Technol Lett 31: 429–435, 2001 © 2002 Wiley Periodicals, Inc., 33: 148, 2002.
DOI 10.1002/mop.10257

The correct information for authors in [1] is as given above. In this article, the following four equations should be corrected to

$$\underline{f}_n^{\pm}(\underline{r}) = \begin{cases} \dfrac{l_n}{2A_n^{\pm}}\rho_n^{\pm}, & \underline{r} \in T_n^{\pm} \\ 0, \quad - & \underline{r} \notin T_n^{\pm} \end{cases}, \tag{15}$$

$$A_m(t_i) + \Delta t(1-\nu)\phi_m(t_i) = \Delta t V_m(t_{i-\nu}) + A_m(t_{i-1}) - \Delta t\nu\phi_m(t_{i-1}), \tag{17}$$

$$\phi_{mn}^{pq} = \frac{1}{4\pi\varepsilon}\int_S \nabla\cdot\underline{f}_m^p(\underline{r})\int_S \frac{\nabla'\cdot\underline{f}_n^q(\underline{r}')}{R}\,dS'\,dS, \tag{24}$$

and

$$\beta_m = \Delta t V_m(t_{i-\nu}) + A_m(t_{i-1}) - \lfloor \tilde{A}_m(t_i) - \dot{P}_m(t_{i-1})\rfloor - \Delta t\nu\phi_m(t_{i-1}) - \Delta t(1-\nu)\lfloor \tilde{\phi}_m(t_i) + \dot{B}_m(t_{i-1}) + \dot{D}_m(t_{i-2})\rfloor. \tag{48}$$

The correct caption for Figure 7 is as follows: Figure 7. Triangle patching of a conducting sphere with radius 0.5 m. 168 patches, 252 common edges.

## REFERENCE

1. B.H. Jung and T.K. Sarkar, Time-domain electric-field integral equation with central finite difference, Microwave Opt Technol Lett 31 (2001), 429–435.